
Chapter 6: Paleoclimate

1
2
3
4
5
6
7
8
9
10
11
12
13
14
15
16
17
18
19
20
21
22
23
24

Coordinating Lead Authors:

Eystein Jansen, Jonathan Overpeck

Lead Authors:

Keith R. Briffa, Jean-Claude Duplessy, Fortunat Joos, Valérie Masson-Delmotte, Daniel O. Olago, Bette Otto-Bliesner, Wm. Richard Peltier, Stefan Rahmstorf, Rengaswamy Ramesh, Dominique Raynaud, David H. Rind, Olga Solomina, Ricardo Villalba, De'er Zhang.

Contributing Authors:

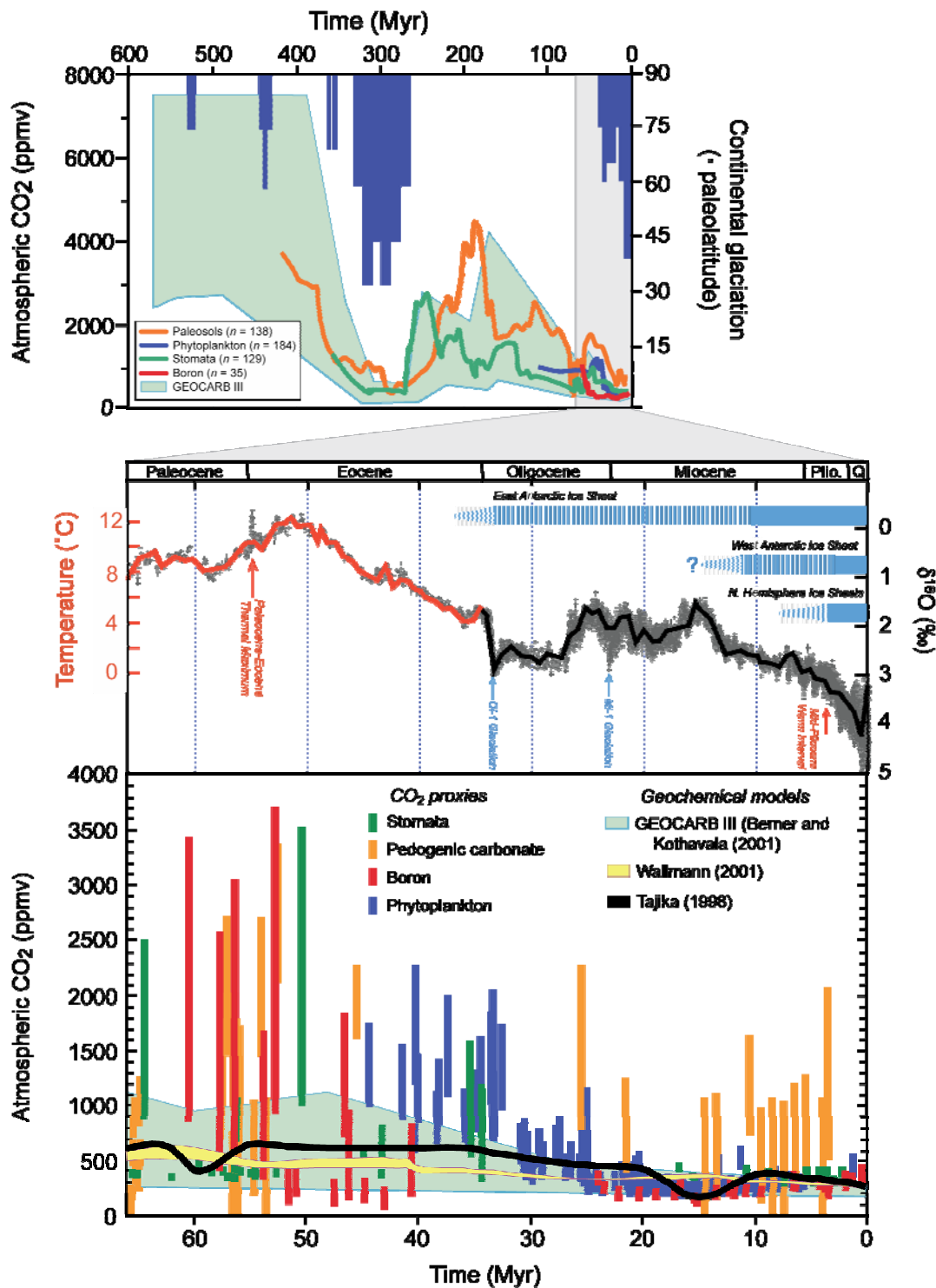
Jean-Marc Barnola, Eva Bauer, Mark Chandler, Julia Cole, Edward R. Cook, Elsa Cortijo, Trond Dokken, Dominik Fleitmann, Myriam Khodri, Laurent Labeyrie, Anders Levermann, Øyvind Lie, Marie-France Loutre, Erik Monnin, Daniel Muhs, Tim Osborn, Frederic Parrenin, Gian-Kasper Plattner, Henry N. Pollack, Øyvind Paasche, Lowell Stott, Ellen Mosley-Thompson, Renato Spahni, Guo-Zheng-Tang, Lonnie Thompson, Claire Waelbroeck, Jim Zachos.

Review Editors: Jean Jouzel, John Mitchell

Date of Draft: 7 March 2006

Notes: TSU compiled version

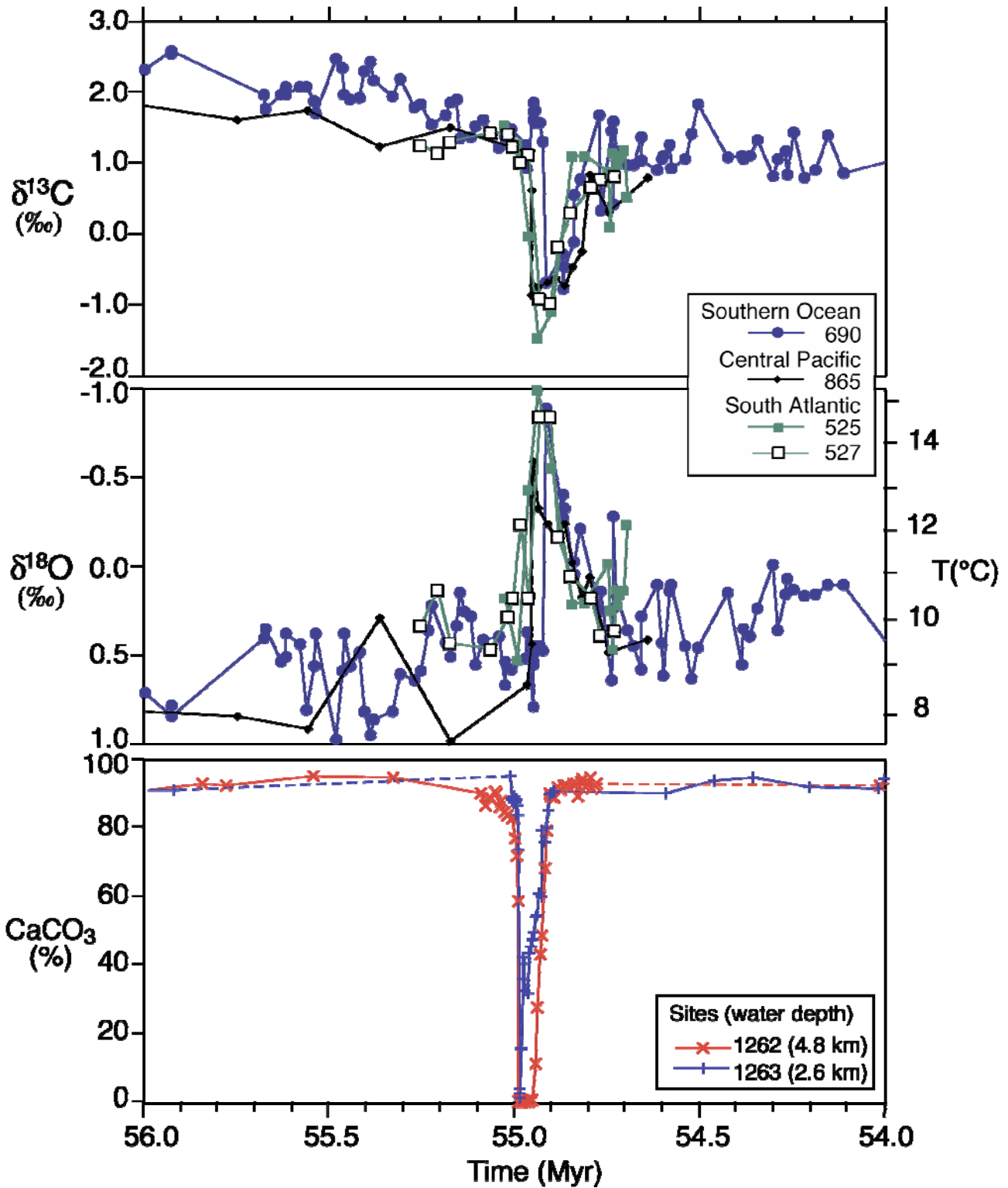
1
2
3



4
5 **Figure 6.1.** Top panel: Records of atmospheric CO₂ and continental glaciation for the Phanerozoic Eon (542
6 Myr ago to present). Vertical blue bars mark the timing and paleolatitudinal extent of continental glaciations
7 (after Crowley, 1998). The plotted CO₂ records represent five-point running averages of CO₂ reconstructions
8 from each of the four major proxies (see Royer, in press for details of compilation). Also plotted are the
9 plausible ranges of CO₂ predictions from the geochemical carbon cycle model GEOCARB III (Berner and
10 Kothavala, 2001). All data have been adjusted to the Gradstein et al. (2004) timescale.
11 Middle panel: The global compilation of deep sea benthic foraminifera oxygen isotope records from 40
12 DSDP and ODP sites (Zachos et al., 2001) updated with the addition of high-resolution records for the
13 interval spanning the Eocene through Miocene (Billups et al., 2002; Bohaty and Zachos, 2003; Lear et al.,
14 2004). Most data were derived from analyses of two common and long-lived benthic taxa, *Cibicidoides* and

1 *Nuttallides*. To correct for genus-specific isotope vital effects, the ^{18}O values were adjusted by +0.64 and
2 +0.4 (Shackleton et al., 1984), respectively. The ages are relative to the GPTS of Berggren et al. (1995). The
3 raw data were smoothed using a five-point running mean, and curve-fitted with a locally weighted mean. The
4 ^{18}O temperature scale was computed assuming an ice-free ocean [~ 1.2 Standard Mean Ocean Water
5 (SMOW)], and thus only applies to the time preceding the onset of large-scale glaciation on Antarctica (~ 35
6 Myr ago). From that time (early Oligocene) to the present, much of the variability ($\sim 70\%$) in the ^{18}O record
7 reflects changes in Antarctica and Northern Hemisphere ice volume. The presumption of a negligible
8 contribution from ice sheets prior to about 35 Myr ago, and large ice-sheets thereafter, is supported by
9 several lines of evidence, including the distribution of glaciomarine sediment or ice-rafted debris near or on
10 Antarctica, and by changes in the distribution and abundances of clay minerals associated with physical
11 weathering in proximal margin and deep-sea sediments (e.g., Hambrey et al., 1991; Wise et al., 1991;
12 Ehrmann and Mackensen, 1992). The horizontal bars (shown in light blue) provide a qualitative
13 representation of ice volume in Northern Hemisphere and Antarctic ice sheets. The dashed bars represent
14 periods of partial or ephemeral ice, while the solid bars represent ice sheets of modern or greater size. The
15 evolution and stability of the West Antarctic ice sheet (e.g. Lemasurier and Rocchi, 2005) remains an
16 important area of uncertainty that could impact estimates of future sea level rise.
17 Bottom panel: Detailed record of CO_2 for the last 65 Myr. Individual records of CO_2 and associated errors
18 are color-coded by proxy method; when possible, records are based on replicate samples (see Royer, in press
19 for details). Error terms for age are typically $< \pm 1$ Myr. Also plotted are the plausible ranges of CO_2
20 predictions from three geochemical carbon cycle models.
21

1
2

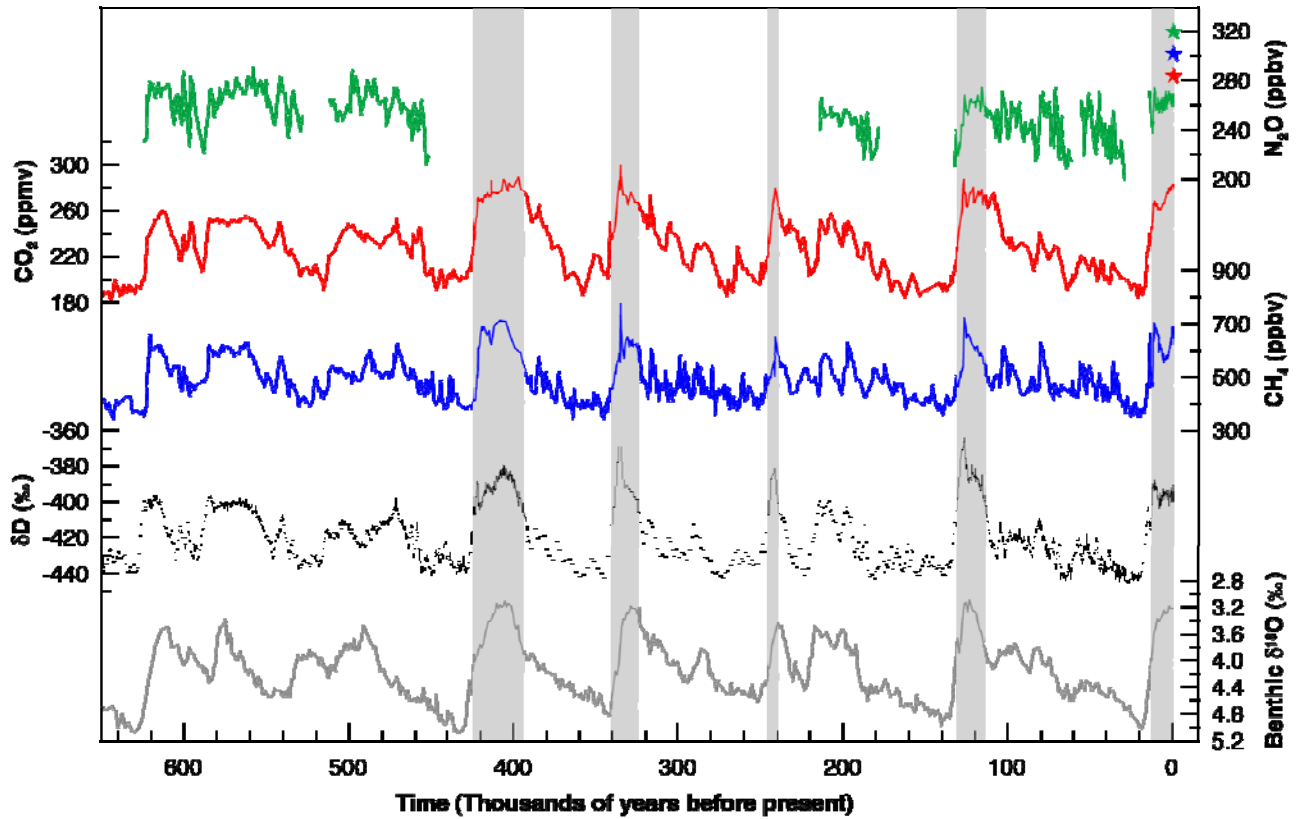


3
4
5
6
7
8
9
10
11
12

Figure 6.2. The Paleocene-Eocene Thermal Maximum (PETM) as recorded in benthic (bottom dwelling) foraminifer (*N. truempyi*) isotopic records from sites in the Antarctic, south Atlantic and Pacific (see Zachos et al., 2003 for details). The rapid decrease in carbon isotope ratios in the top panel is indicative of a large increase in atmospheric greenhouse CO_2 and CH_4 , that was coincident with $\sim 5^\circ\text{C}$ global warming (center panel). Using the carbon isotope records, numerical models show that CH_4 released by the rapid decomposition of marine hydrates might have been a major component (~ 2000 GtC) of the carbon flux (Dickens and Owen, 1996). Testing of this and other models requires an independent constraint on the carbon fluxes. In theory, the much of the additional greenhouse carbon would have been absorbed by the

1 ocean, thereby lowering seawater pH and causing widespread dissolution of seafloor carbonates. Such a
2 response is evident in the lower panel which shows a transient reduction in the carbonate content of
3 sediments in two cores from the south Atlantic (Zachos et al., 2004; Zachos et al., 2005). The observed
4 patterns indicate that the oceans carbonate saturation horizon rapidly shoaled over 2 km, and then gradually
5 recovered as buffering processes slowly restored the chemical balance of the ocean. Initially, most of the
6 carbonate dissolution is of sediment deposited prior to the event, a process that offsets the apparent timing of
7 the dissolution horizon relative to the base of the benthic foraminifer carbon isotope excursion. Model
8 simulations show that the recovery of the carbonate saturation horizon should precede the recovery in the
9 carbon isotopes by as much as 100 kyr (Dickens and Owen, 1996), another feature that is evident in the
10 sediment records.

1
2



3
4
5
6
7
8
9
10
11
12
13
14
15
16
17

Figure 6.3. Variations of deuterium in Antarctic ice, a proxy for local temperature, and the atmospheric concentrations of the greenhouse gases carbon dioxide, methane, and nitrous oxide derived from air trapped within ice cores from Antarctica and from recent atmospheric measurements (Petit et al., 1999; Indermühle et al., 2000; EPICA community members, 2004; Spahni et al., 2005; Siegenthaler et al., 2005b). The shading indicates the last interglacial warm periods. There is clear evidence for interglacial periods prior to 450,000 years, but these were apparently colder than the typical interglacials of the latest Quaternary. The length of the current interglacial is not unusual in the context of the last 650,000 years. The stack of 57 globally distributed benthic $\delta^{18}\text{O}$ marine records, a proxy for global ice volume fluctuations (Lisiecki and Raymo, 2005), is displayed in the bottom part of the figure for comparison with the ice core data. Larger ice volume is expressed downwards. Note that the shaded vertical bars are based on the ice core age model (EPICA community members, 2004), and that the marine record is plotted on its original time scale based on tuning to the orbital parameters (Lisiecki and Raymo, 2005).

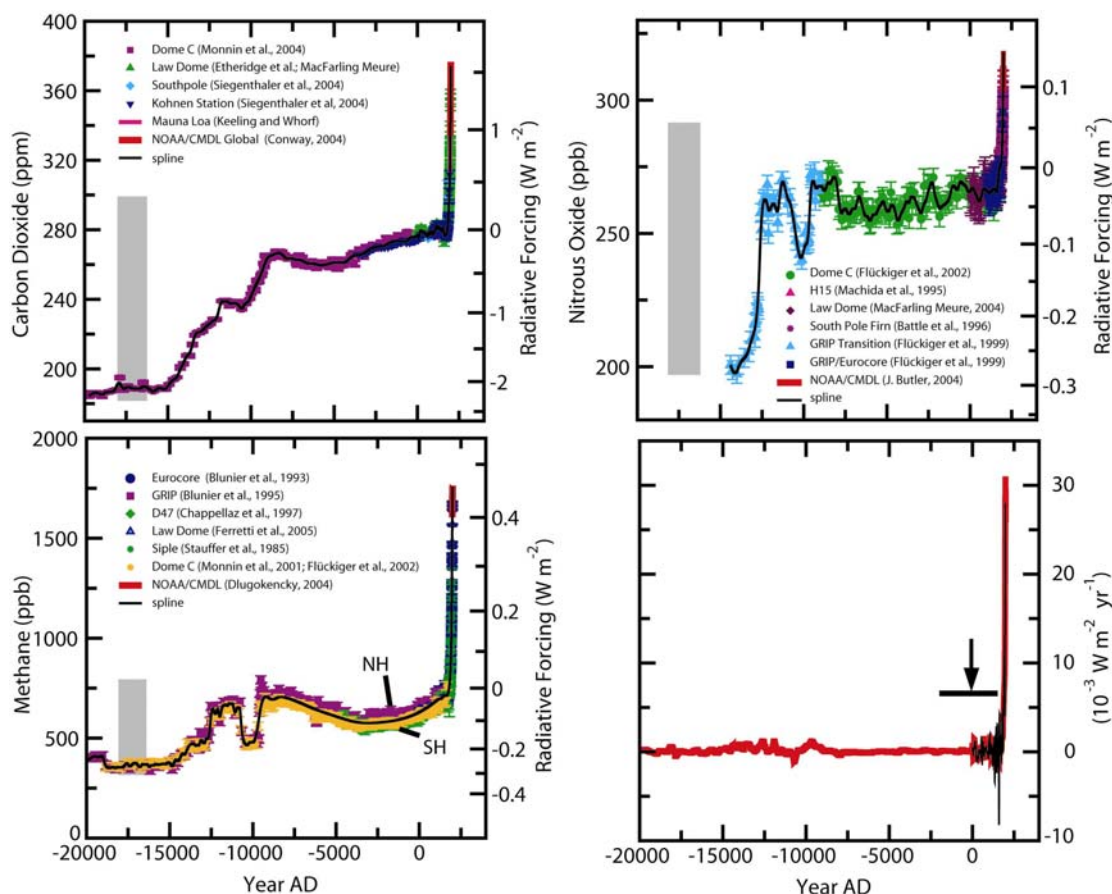
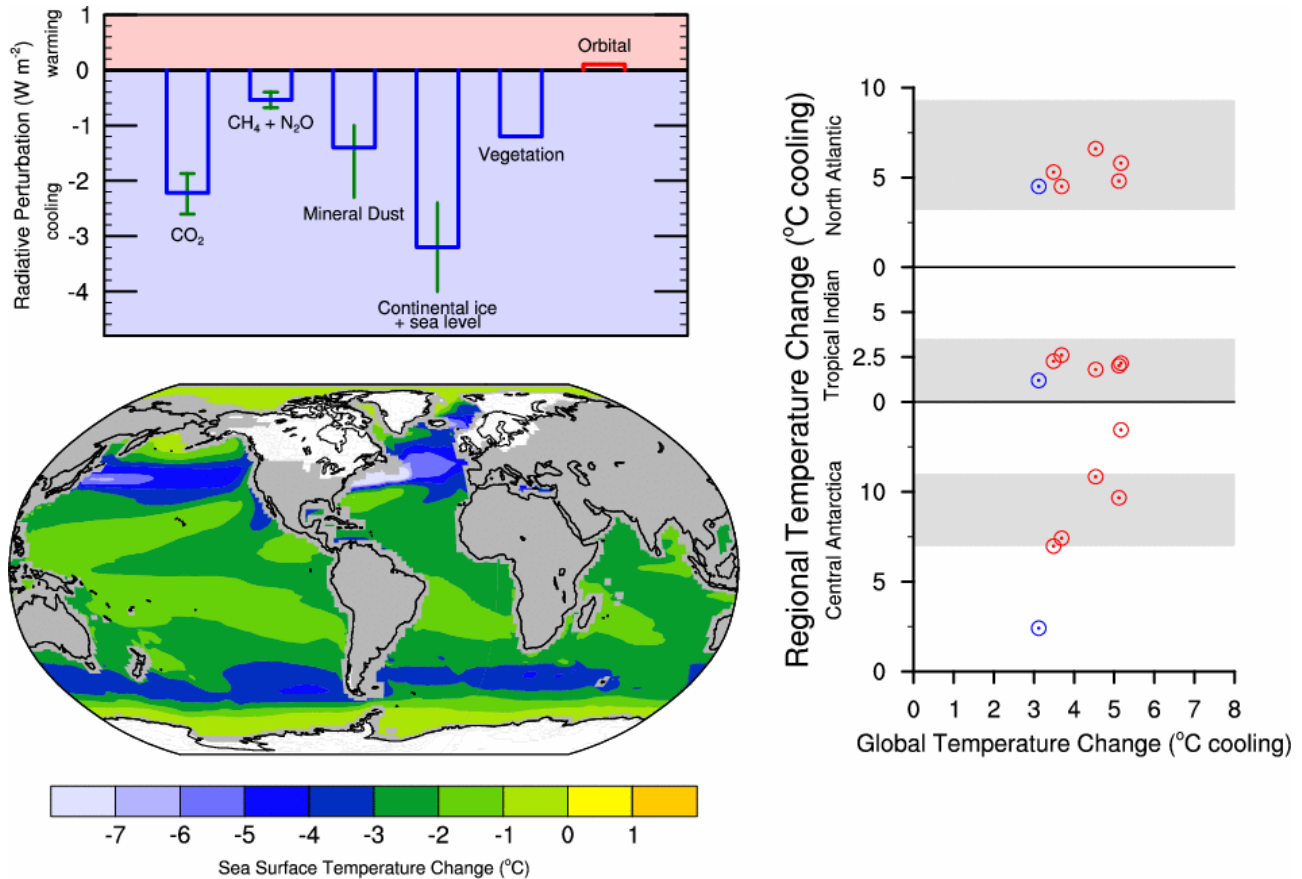
1
23
4
5
6
7
8
9
10
11
12
13
14
15
16
17
18
19
20
21
22
23
24
25
26

Figure 6.4. The concentrations and radiative forcing by (a) carbon dioxide (CO_2), (b) methane (CH_4), (c) nitrous oxide (N_2O), and (d) the rate of change in their combined radiative forcing over the last 20,000 years reconstructed from Antarctic and Greenland ice and firn data (symbols) and direct atmospheric measurements (red and magenta lines). The grey ranges show the reconstructed ranges of natural variability for the past 650,000 years (Siegenthaler et al., 2005b; Spahni et al., 2005). Radiative forcing has been computed with the simplified expressions of chapter 2 (Myhre et al., 1998). The rate of change in radiative forcing (red line) has been computed from spline fits (Enting, 1987) of the concentration data (thin black lines in panel a-c). The width of the age distribution of the bubbles in ice varies from ~ 20 years for sites with a high accumulation of snow such as Law Dome, Antarctica, to ~ 200 years for low accumulation sites such as Dome Concordia, Antarctica. The Law Dome ice and firn data, covering the past two millennia, have been splined with a cut-off period of 40 years and the resulting rate of change in radiative forcing is shown by the thin black line in d. The arrow indicates how the anthropogenic peak would have been recorded in ice during the last glacial transition. It shows the peak in the rate of change in radiative forcing after the anthropogenic signals of CO_2 , CH_4 , and N_2O have been smoothed with a model describing the enclosure process of air in ice (Spahni et al., 2003) applied for conditions at the low accumulation Dome Concordia site. The CO_2 data are from (Etheridge et al., 1996; Monnin et al., 2001; MacFarling Meure, 2004; Monnin et al., 2004; Siegenthaler et al., 2005a), the CH_4 data from (Stauffer et al., 1985; Steele et al., 1992; Blunier et al., 1993; Dlugokencky et al., 1994; Blunier et al., 1995; Chappellaz et al., 1997; Monnin et al., 2001; Flückiger et al., 2002; Ferretti et al., 2005), the N_2O data from (Machida et al., 1995; Battle et al., 1996; Flückiger et al., 1999; Flückiger et al., 2002; MacFarling Meure, 2004). Atmospheric data are from the NOAA global air sampling network, representing global average concentrations (Steele et al., 1992; Dlugokencky et al., 1994), and from Mauna Loa, Hawaii (Keeling and Whorf, 2005).

1
2

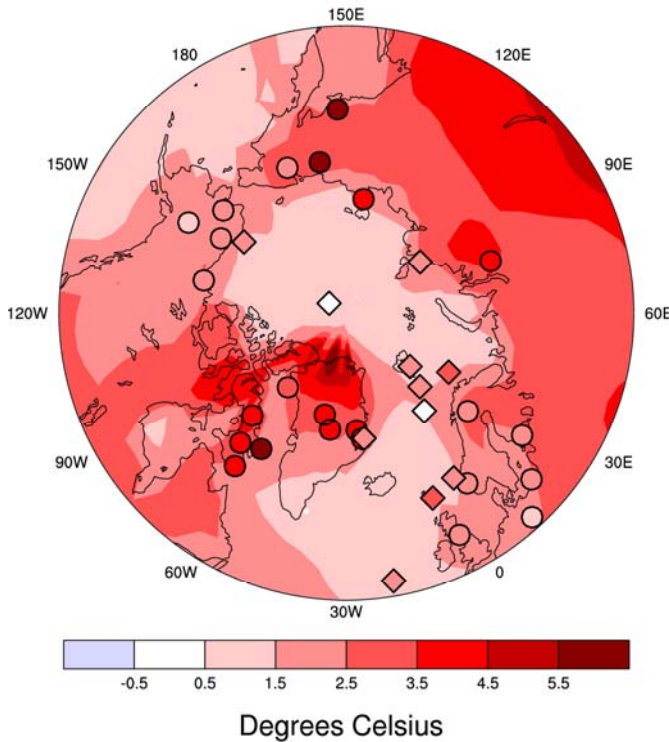


3
4
5
6
7
8
9
10
11
12
13
14
15
16
17
18
19
20
21
22
23

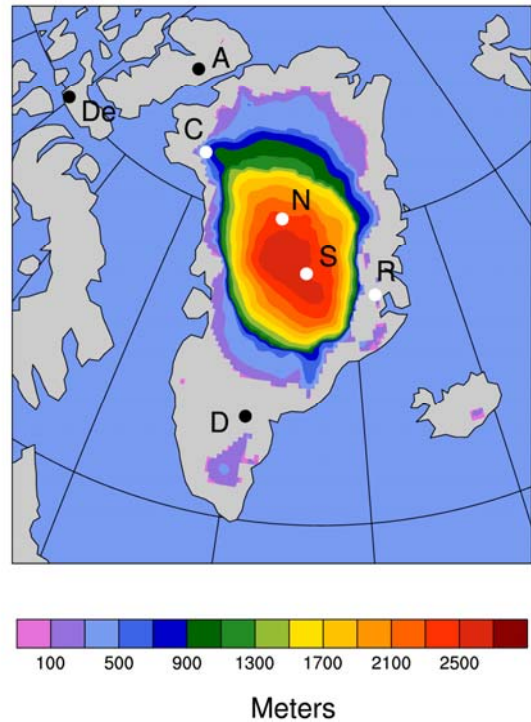
Figure 6.5. The Last Glacial Maximum (around 21kyrs ago) relative to pre-industrial (1750). See text for more details and references. Top left: Global annual mean radiative influences ($W m^{-2}$) of LGM climate change agents, generally feedbacks on glacial-interglacial cycles but specified in most AOGCM simulations for LGM. The heights of the rectangular bars denote best estimate values guided by published values of the forcing and physical understanding. Vertical lines about rectangular bars are ranges as follows: greenhouse gases include uncertainties in ice core measurements and errors in simplified expressions for converting concentrations to radiative perturbations (see Chapter 2); mineral dust aerosols include range of estimates from modeling studies of direct effects only; continental ice sheets/sea level is range of PMIP-2 AOGCMs, all using prescribed ICE-5G ice sheet and does not include uncertainties of LGM ice sheet extent or height. No range is available for LGM vegetation changes. Bottom left: Multi-model average SST change for LGM PMIP-2 simulations by five AOGCMs (CCSM, FGOALS, HadCM, IPSL, and MIROC). Ice extent over continents is shown in white. Right: LGM regional cooling as compared to LGM global cooling as simulated in PMIP-2, AOGCM results shown as red circles, EMIC (ECBilt-CLIO) result shown as blue circle. Regional averages are defined as Antarctica, annual for inland ice cores; tropical Indian Ocean, annual for $15^{\circ}S-15^{\circ}N, 50-100^{\circ}E$; North Atlantic Ocean, July-August-September for $42-57^{\circ}N, 35^{\circ}W-20^{\circ}E$. Grey shading indicates range of proxy estimates of regional cooling: Antarctica (Stenni et al., 2001), tropical Indian Ocean (Barrows and Juggins, 2005), North Atlantic Ocean (Rosell-Mele et al., 2004; deVernal et al., 2005; Kucero and al., 2005).

1
2

Summer Surface Temperature Change



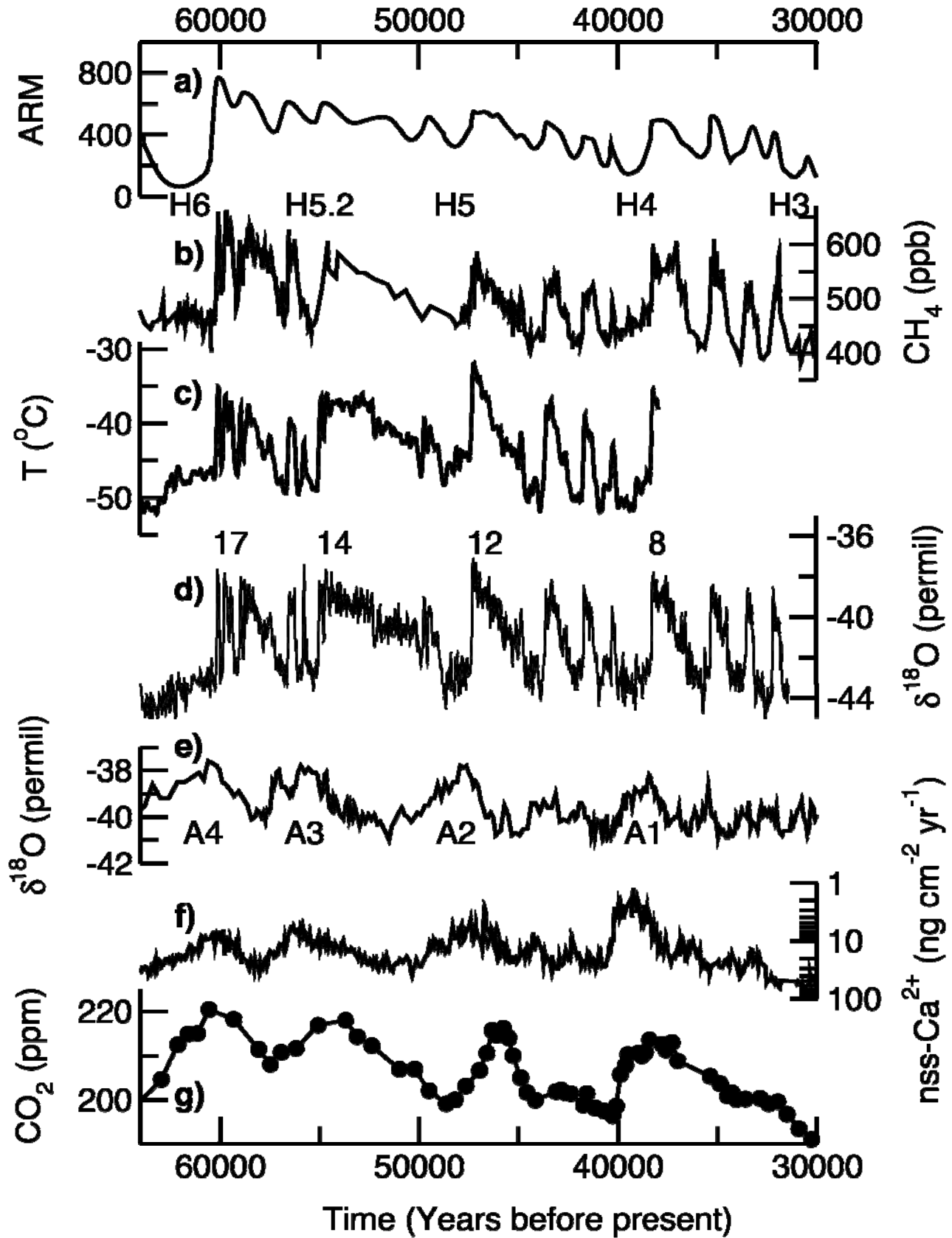
Ice Thickness



3
4
5
6
7
8
9
10
11
12
13
14
15
16
17

Figure 6.6. Summer surface air temperature change over the Arctic and annual ice thickness and extent for Greenland and western Arctic glaciers for the Last Interglacial (at approximately 130–125 kyr ago) from a multi-model and a multi-proxy synthesis. The summer warming simulated by the NCAR CCSM (Otto-Bliesner et al., 2006) and ECHO-G model (Kaspar et al., 2005) is contoured in the left panel and is overlain by proxy estimates of maximum summer warming from terrestrial (circles) and marine (diamonds) sites as compiled in the syntheses published by the CAPE Project Members (2006) and Kaspar et al. (2005). Extents and thicknesses of the Greenland ice sheet and western Canadian and Iceland glaciers are shown at their minimum extent for the Last Interglacial as a multi-model average from three ice models (Tarasov and Peltier, 2003; Lhomme et al., 2005b; Otto-Bliesner et al., 2006). Ice core observations (Koerner, 1989; North Greenland Ice Core Project, 2004) indicate Last Interglacial ice (white dots) at Renland (R), NGRIP (N), Summit (S, GRIP and GISP2), and possibly Camp Century (C), but no LIG ice (black dots) at Dye-3 (D), Devon (De), and Agassiz (A).

1
2

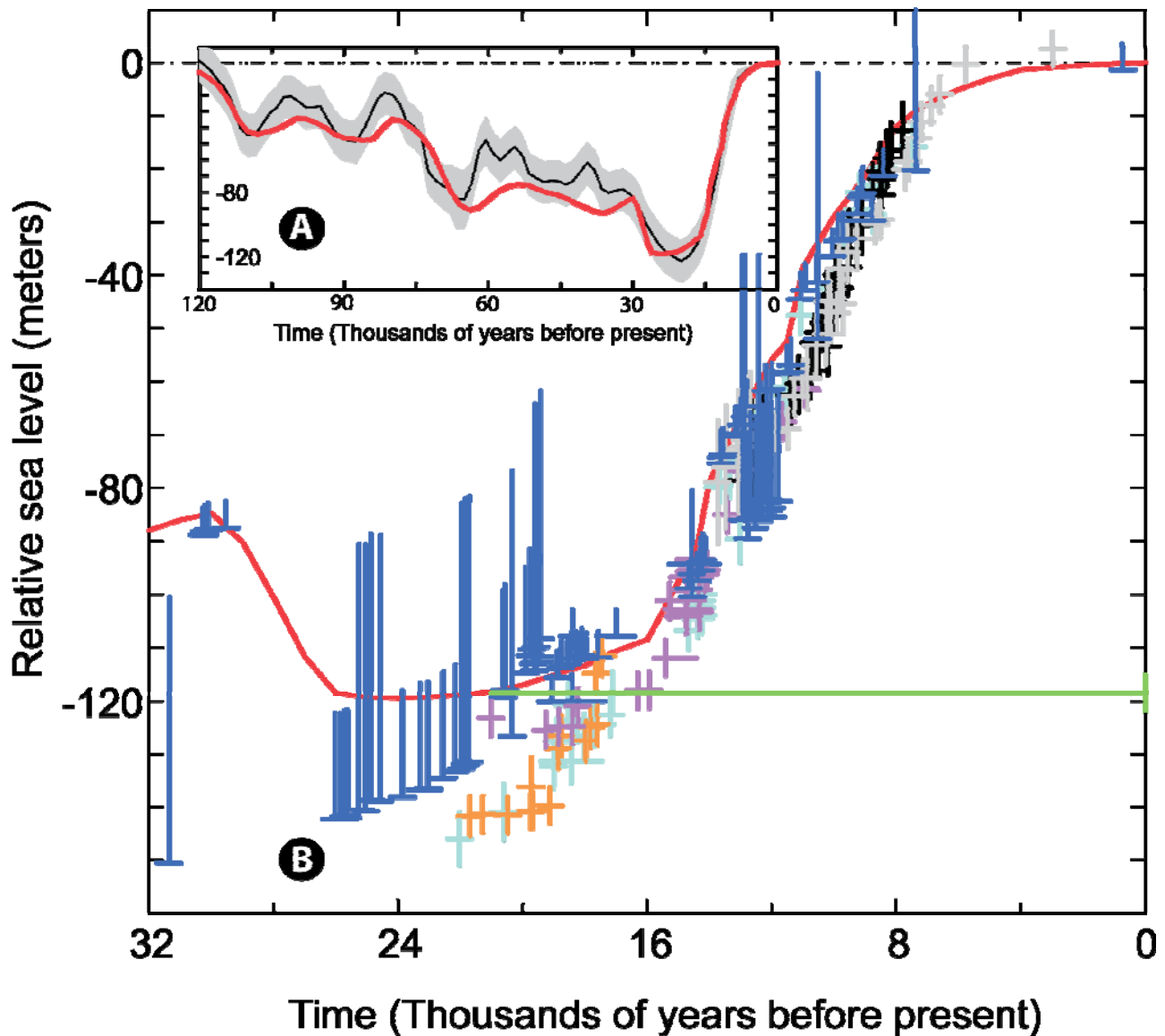


3
4
5
6
7
8

Figure 6.7. The evolution of climate indicators from the Northern Hemisphere (panels a to d) and from Antarctica (panels e to f) over the period 64,000 to 30,000 years before present. a) Anhyseretic remanent magnetisation (ARM), here a proxy of the northward extent of Atlantic Meridional Overturning circulation, from an ocean sediment core from the Nordic Seas (Dokken and Jansen, 1999); b) methane as recorded in

1 Greenland ice cores at the GRIP, GISP (data from 40 to 64 thousand years ago), and NorthGRIP sites
2 (Blunier and Brook, 2001; Flückiger et al., 2004; Huber et al., 2006). CH₄ data for the period 40 to 30
3 thousand years ago were selected for the GRIP site and for 64 to 40 thousand years ago for the GISP site
4 when sample resolution is highest in the cores; c) surface temperature estimated from nitrogen isotope ratios
5 that are influenced by thermal diffusion (Huber et al., 2006); d) $\delta^{18}\text{O}$, a proxy for surface temperature, from
6 NorthGRIP (North Greenland Ice Core Project, 2004); e) $\delta^{18}\text{O}$ from Byrd, Antarctica (Blunier and Brook,
7 2001); f) nss-Ca²⁺, a proxy of dust and iron deposition, from Dome C, Antarctica (Röthlisberger et al., 2004);
8 g) CO₂ as recorded in ice from Taylor Dome, Antarctica (Indermühle et al., 2000). The Dansgaard/Oeschger
9 Northern Hemisphere warm events 8, 12, 14, and 17, the Heinrich events, periods of massive ice rafted
10 debris recorded in marine sediments, H3, H4, H5, H5.2, and H6, as well as the Antarctic warm events A1 to
11 A4 are shown. All data are plotted on the Greenland SS09sea time scale. CO₂ and CH₄ are well mixed in the
12 atmosphere. CH₄ variations are synchronous (within the resolution of ± 50 years) with variations in
13 Greenland temperature. CO₂ co-varied with the Antarctic temperature (The exact synchronisation between
14 Taylor Dome and Byrd is not without uncertainties making the determination of lead or lags between
15 temperature and CO₂ elusive). The evolution of Greenland and Antarctic temperature is consistent with a
16 reorganisation of the heat fluxes and the Meridional Overturning Circulation in the Atlantic (Knutti et al.,
17 2004).
18

1
2

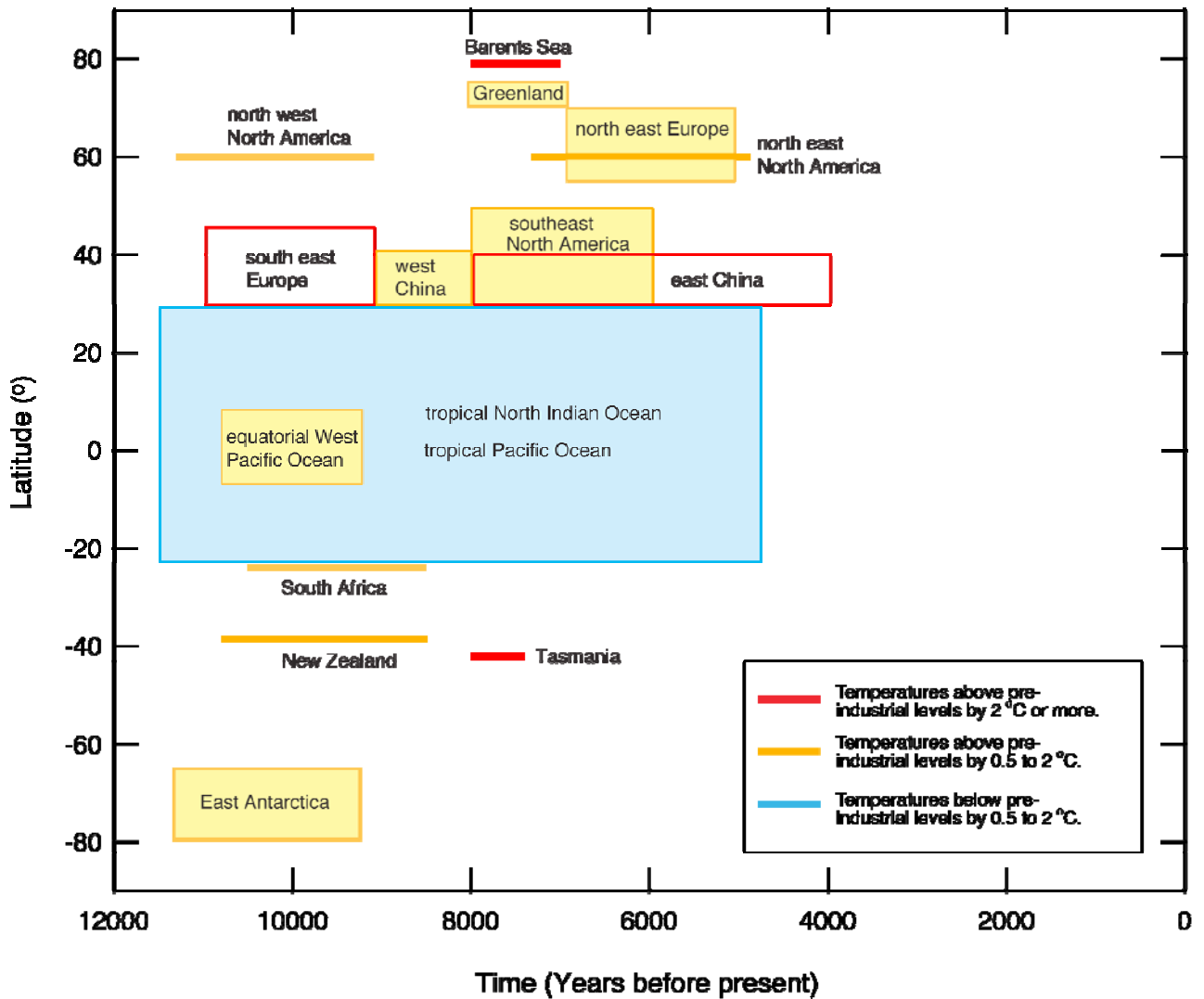


3
4
5
6
7
8
9
10
11
12
13
14
15
16
17
18
19
20
21
22
23

Figure 6.8. (a) The ice equivalent eustatic sea level history over the last glacial-interglacial cycle according to the reconstruction of Waelbroeck et al. (2002). The black line defines the mid-point of their estimates for each age and the surrounding hatched region an estimate of error. The red line is the prediction of the ICE-5G(VM2) model for the Barbados location for which the relative sea level observations themselves provide a close approximation to the ice equivalent eustatic sea level curve.

(b) The fit of the ICE-5G(VM2) model prediction (red line) to the coral based record of relative sea level history from the island of Barbados in the Caribbean Sea (Fairbanks, 1989; Peltier and Fairbanks, accepted) over the age range from the present day to 30,000 years before present. The individual coral based estimates of relative sea level (blue) have an attached error bar that depends upon the coral species. The estimates denoted by the short error bars are derived from the *Acropora Palmata* species which provide the tightest constraints upon relative sea level as this species is found to live within approximately 5m of sea level in the modern ecology. The estimates denoted by the longer error bars are derived either from the *Monastrea Annularis* species of coral (error bars of intermediate length) or from further species which are found over a wide range of depths with respect to sea level (longest error bars). These data are most useful in providing a lower bound for the sea level depression. The data denoted by the colored crosses are from the ice equivalent eustatic sea level reconstruction of Lambeck and Chappell (2001). The color code employed for these data is as follows: cyan (Barbados), grey (Tahiti), black (Huon), orange (Bonaparte Gulf), purple (Sunda Shelf). The green line denotes the conventionally inferred LGM sea level lowering of 120 m (eg. Shackleton, 2000)

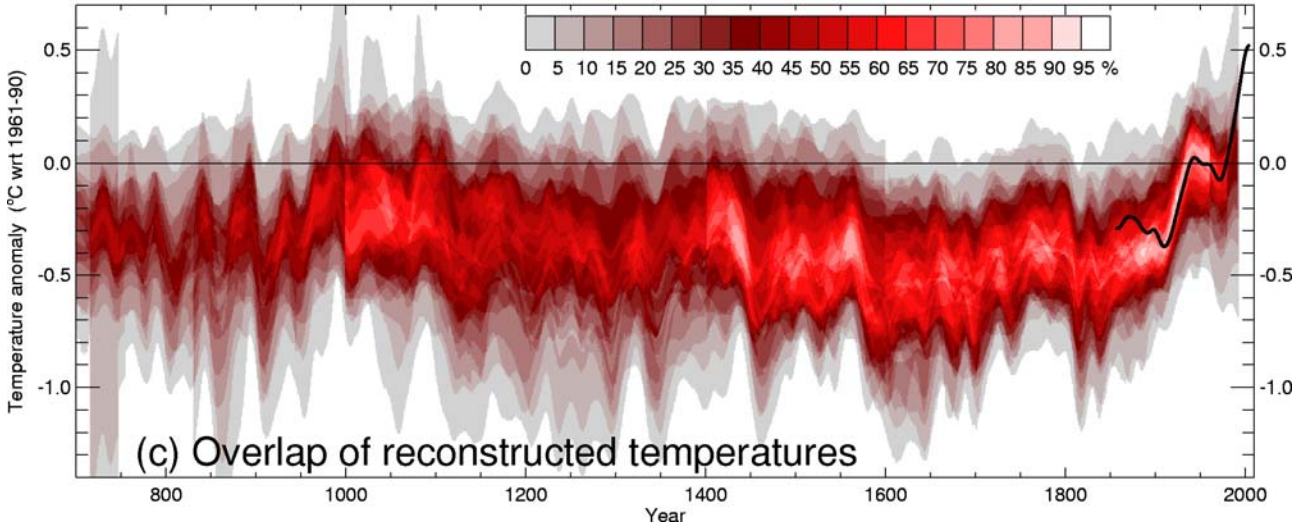
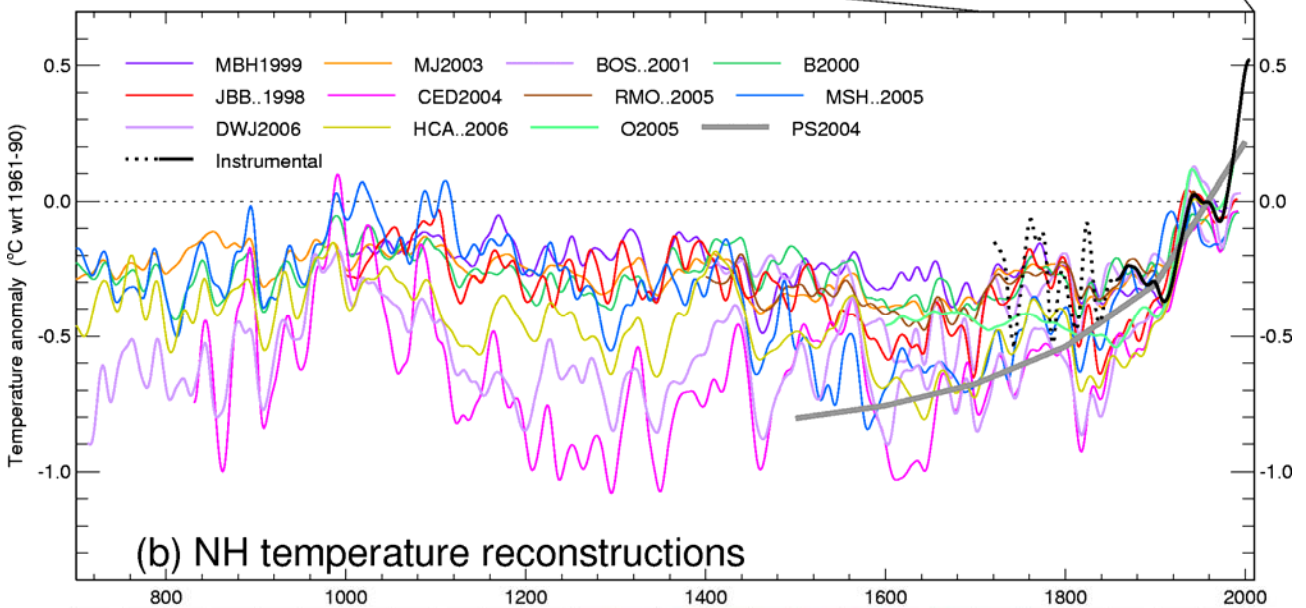
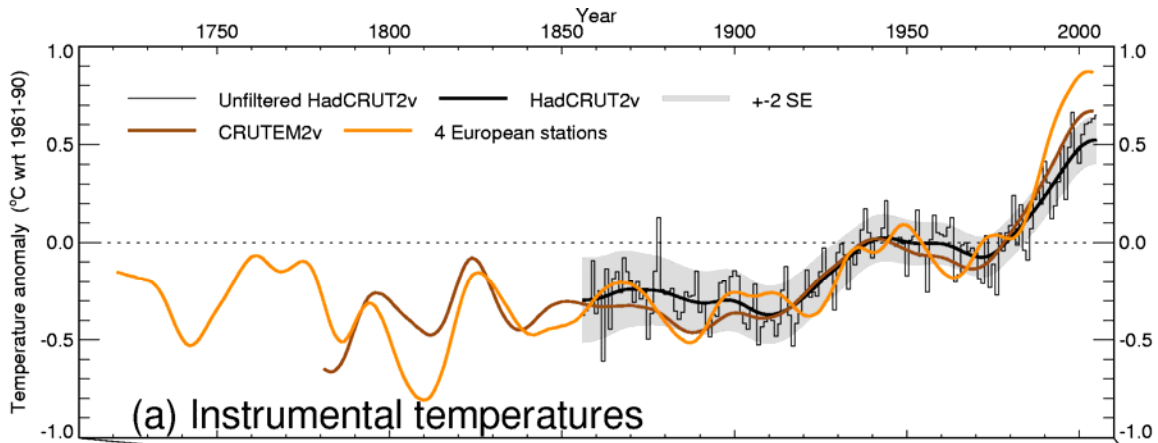
1
2



3
4
5
6
7
8
9
10
11
12
13
14

Figure 6.9. Timing and intensity of maximum temperature deviation from pre-industrial levels, as a function of latitude (vertical axis) and time (horizontal axis, in thousands of years before present, 1950 A.D.). Temperatures above pre-industrial levels by 0.5°C to 2°C appear in orange (above 2°C in red). Temperatures below pre-industrial levels by 0.5°C to 2°C appear in blue. References for datasets are : Barents Sea (Duplessy et al., 2001), Greenland (Johnsen et al., 2001), Europe (Davis et al., 2003), northwest and northeast America (Kaufman et al., 2004) (MacDonald et al., 2000), China (He et al., 2004), tropical oceans (Rimbu et al., 2004) (Stott et al., 2004) (Lorentz et al., 2006), north Atlantic (Marchal et al., 2002) (Kim et al., 2004), Tasmania (Xia et al., 2001), East Antarctica (Masson et al., 2000), south Africa (Holmgren et al., 2003), New Zealand (Williams et al., 2004).

1
2



3
4
5
6
7
8
9
10

Figure 6.10. Records of Northern Hemisphere temperature variation during the last 1300 years. (a) Annual-mean instrumental temperature records: black = land and marine temperatures for the full NH (series [I1] in Table 6.1), with annual values (thin line) and ± 2 standard errors ([I2], grey shading); brown = land only temperatures for the NH [I3]; orange = average of temperatures from 4 stations in Europe [I4]. (b) Reconstructions using multiple climate proxy records: red (JBB..1998) = [R1]; dark purple (MBH1999) = series [R2]; light blue (BOS..2001) = [R3]; pink (CED2004) = [R4]; green (B2000) = [R5]; orange

1 (MJ2003) = [R6]; brown (RMO..2005) = [R7]; dark blue (MSH..2005) = [R8]; light purple (DWJ2006) =
2 [R9]; yellow (HCA..2006) = [R10]; thick grey (PS2004) = [R11]; black (Instrumental) = composite of [I4]
3 and [I3] (dotted) and [I1] (solid).

4 (c) Composite of series [R1] to [R12] (excluding [R7] and [R11]) and their published uncertainty ranges
5 indicating the number of overlapping reconstructions (regions within the ± 1 standard error [SE] of a
6 reconstruction score 10%, regions within ± 2 SE score 5%; maximum 100% obtained for temperatures that
7 fall within ± 1 SE of all 10 reconstructions). Series [I1] is shown in black.

8
9 All series have been smoothed with a Gaussian-weighted filter to remove fluctuations on time scales less
10 than 30 years; smoothed values are obtained up to both ends of each record by extending the records with the
11 mean of the adjacent existing values. All temperatures represent anomalies ($^{\circ}\text{C}$) from the 1961–1990 mean.
12